Reduced particle and heat transport with quasisymmetry in the Helically Symmetric Experimenta)

J. M. Canik, D. T. Anderson, F. S. B. Anderson, C. Clark, K. M. Likin, J. N. Talmadge, and K. Zhai

Citation: Physics of Plasmas **14**, 056107 (2007); doi: 10.1063/1.2709862
View online: http://dx.doi.org/10.1063/1.2709862
View Table of Contents: http://scitation.aip.org/content/aip/journal/pop/14/5?ver=pdfcov
Published by the AIP Publishing

Reduced particle and heat transport with quasisymmetry in the Helically Symmetric Experiment[a)]

J. M. Canik,[b)] D. T. Anderson, F. S. B. Anderson, C. Clark, K. M. Likin, J. N. Talmadge, and K. Zhai
Department of Electrical and Computer Engineering, University of Wisconsin-Madison, Madison, Wisconsin 53706

(Received 3 November 2006; accepted 25 January 2007; published online 13 April 2007)

Measurements of particle and heat transport have been made in the Helically Symmetric Experiment [F. S. B. Anderson *et al.*, Fusion Technology **27**, 273 (1995)]. Experimental differences in the density and temperature profiles are reported between plasmas produced in a quasihelically symmetric (QHS) magnetic field and a configuration with the symmetry broken. The electron temperature is higher in the QHS configuration, due to a reduction in electron thermal diffusivity that is comparable to the neoclassical prediction. The density profile in plasmas with the symmetry broken is measured to be hollow, while in QHS plasmas the profile is centrally peaked. Calculations of the radial particle flux using the DEGAS code [D. Heifetz *et al.*, J. Comput. Phys. **46**, 309 (1982)] show that the hollow profile observed with the symmetry broken is due to neoclassical thermodiffusion. Thermodiffusion is reduced in the QHS configuration, resulting in a peaked density profile. © *2007 American Institute of Physics*. [DOI: 10.1063/1.2709862]

I. INTRODUCTION

Stellarators are attractive candidates as fusion reactors because the confining fields are produced by currents flowing in external conductors. Since externally driven plasma currents are not necessary for confinement, stellarators are inherently steady-state, and can also be free of disruptions. Historically, however, stellarators have had the disadvantage of high neoclassical transport at low collisionality. This large transport is due to the asymmetry in the magnetic ripple from a combination of helical and toroidal curvature. As a result, trapped particle orbits can deviate greatly from a magnetic surface. This deviation gives rise to the so-called "$1/\nu$" regime at low collisionality in which the neoclassical transport increases with decreasing collisionality.[1] Another problem stemming from the asymmetry in the magnetic ripple is particles on direct loss orbits that leave the confinement region before colliding. Trapped alpha particles on direct loss orbits in a conventional stellarator fusion reactor may be lost before they thermalize and redeposit their energy into the plasma, and could cause significant wall damage.

A survey of theoretical approaches to reducing neoclassical transport in stellarators was presented by Mynick.[2] Experimentally, several approaches have been tested. One method, referred to as "sigma optimization," is to shift the magnetic surfaces toward the inboard side of the device to decrease the radial drift of trapped particles.[3] This method was shown to be effective in reducing both neoclassical as well as anomalous transport in the Large Helical Device (LHD).[4] The drawback of this approach is that it may result in a reduction of plasma stability due to the formation of a magnetic hill, although evidence of such an instability has so far been lacking. Another technique to minimize neoclassical transport is to rely on the $\mathbf{E}\times\mathbf{B}$ drift due to a large radial electric field to decrease the drift of trapped particles from a flux surface. Such an improvement of confinement was observed on the Wendelstein 7-A stellarator, in which the prompt loss of neutral beam ions led to a large negative electric field.[5] Also, the electron root due to the ambipolarity constraint yields a large positive electric field that can significantly reduce transport.[6] This enhanced confinement regime has been observed on the Compact Helical System,[7] Wendelstein 7-AS,[8] TJ-II,[9] and LHD.[10] The disadvantage of relying on the radial electric field to optimize neoclassical transport in a stellarator is that it has minimal effect on highly energetic alpha particles.

A third method that is now being actively explored is that of quasisymmetry.[11] A quasisymmetric stellarator is one in which the magnitude of the magnetic field is approximately a constant for a given direction. The Helically Symmetric Experiment (HSX)[12] is the first operational stellarator based on this concept, with symmetry in the helical direction. This symmetry was achieved by greatly reducing the toroidal component,[13] while maintaining the other symmetry-breaking components of the magnetic-field spectrum at a low level. Other quasisymmetric configurations being constructed or designed are quasiaxisymmetric (such as the National Compact Stellarator Experiment[14]) and quasipoloidally symmetric (QPS[15]) devices. A fourth method of transport reduction relies on drift optimization without maintaining a direction of quasisymmetry, often referred to as quasi-isodynamic. The Wendelstein 7-X[16] experiment, also under construction, falls into this category.

Previously it had been demonstrated in HSX that the neoclassical parallel viscous damping of plasma flow can be reduced in a quasihelically symmetric stellarator.[17] In this paper, we present the first data to show that the improved neoclassical properties of the quasisymmetric configuration

[a)]Paper ZI1 4, Bull. Am. Phys. Soc. **51**, 336 (2006).
[b)]Invited speaker.

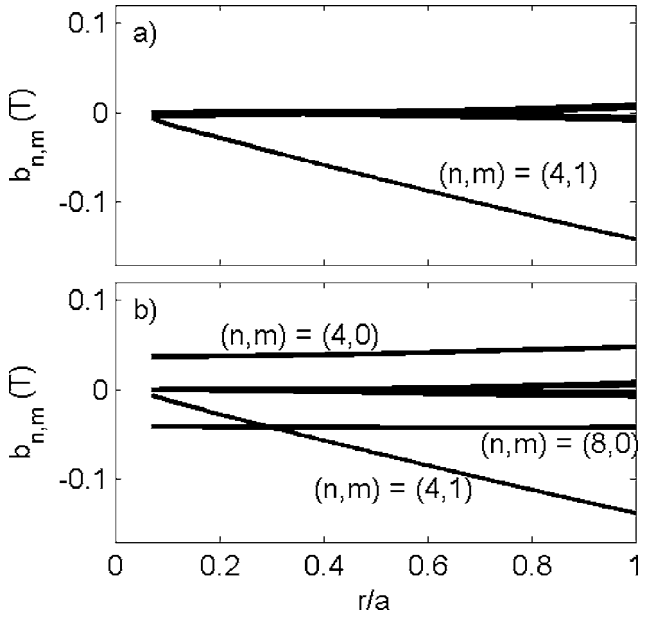

FIG. 1. Magnetic spectrum for the (a) QHS and (b) Mirror configurations.

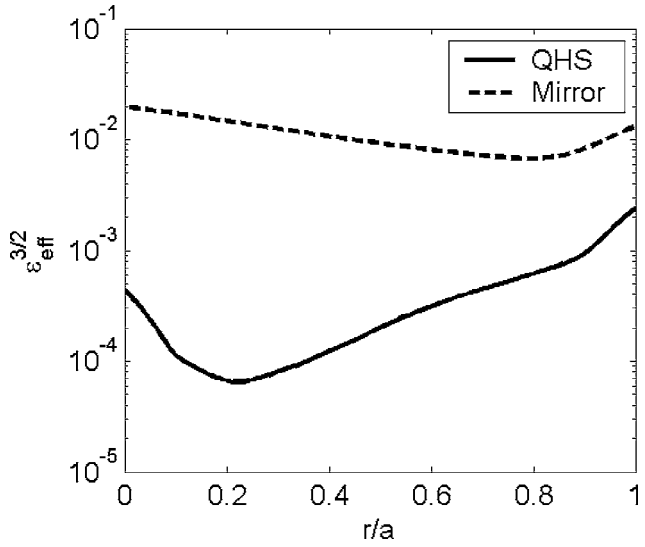

FIG. 2. Profiles of the effective ripple in the QHS (solid line) and Mirror (dashed line) configurations.

can result in significantly reduced particle and heat transport. We demonstrate this improvement in low collisionality confinement by comparing electron density and temperature profiles of plasmas in the quasihelically symmetric magnetic field to those in a configuration in which the symmetry is intentionally broken.

The layout of this paper is as follows. Section II describes the magnetic configurations in which the experiments are performed. Section III describes the methods used to calculate neoclassical transport in the two configurations. In Sec. IV, the measurements of particle transport are presented. Section V presents measurements of electron heat transport. Conclusions are presented in Sec. VI.

II. MAGNETIC GEOMETRY

HSX is a medium size stellarator with four field periods, a major radius of 1.2 m, and an average minor radius of 12 cm. All plasma discharges presented in this paper are produced and heated with up to 100 kW of second-harmonic X-mode electron cyclotron resonance heating (ECRH) at 28 GHz, with a magnetic field of 0.5 T. This heating method gives a maximum electron density of 5×10^{12} cm^{-3}.

The main magnetic field of HSX is quasihelically symmetric (QHS), and is generated by a set of 48 nonplanar, modular coils. The field can be described by the Fourier decomposition of $|B|$ on a magnetic surface,

$$B = B_0 \sum_{n,m} \varepsilon_{n,m} \cos(n\varphi - m\theta), \tag{1}$$

where ϕ is the toroidal and θ the poloidal angle in the Boozer coordinate system.[18] In a quasisymmetric device, the magnetic spectrum is dominated by a single component (or terms with the same helicity). The magnetic spectrum for the QHS configuration of HSX is shown in Fig. 1(a). The spectrum is dominated by a single term with toroidal mode number $n=4$ and poloidal mode number $m=1$, illustrating the quasihelical symmetry.

The quasisymmetry of the HSX magnetic field can be broken using a set of auxiliary coils. Each of the modular coils has an adjacent planar coil, which can be energized in such a way that it either adds to or subtracts from the toroidal field generated by the modular coils. When the auxiliary coils are energized, creating what is called the Mirror configuration, two mirror terms are added to the magnetic spectrum. The mode numbers of these components are $(n=4, m=0)$ and $(n=8, m=0)$, as illustrated in Fig. 1(b).

An important feature of the Mirror configuration is that neoclassical transport can be raised back toward the level of a conventional stellarator, while other magnetic properties are similar to the QHS configuration. The effective ripple ε_{eff} quantifies the level of low-collisionality neoclassical transport due to symmetry breaking terms in the magnetic spectrum; in the $1/\nu$ regime, transport is proportional to $\varepsilon_{\text{eff}}^{3/2}$.[19] Figure 2 shows the effective ripple for the QHS and Mirror configurations that was calculated using a field-line following procedure.[20] It can be seen from the figure that $\varepsilon_{\text{eff}}^{3/2}$ increases by almost two orders of magnitude between the two configurations toward the plasma core. As a figure of merit, the effective ripple itself ε_{eff} at $r/a=2/3$ is often used to quantify the degree of symmetry breaking in a stellarator. At this location, the effective ripple is 0.005 for the QHS and 0.040 for the Mirror. While the effective ripple varies greatly between the two configurations, the rotational transform and the well depth hardly vary at all, as seen in Fig. 3. The plasma volume in the two configurations, defined as the volume enclosed by the last closed flux surface, is also similar: 0.355 m^3 in Mirror and 0.384 m^3 in QHS.

The Mirror configuration being studied here is different from that which has been studied in the past in HSX.[17,21,22] The various nonsymmetric configurations are produced using different distributions of current in the 12 auxiliary coils per field period. This is summarized in Table I, which shows the direction of the current in each of the 12 auxiliary coils in

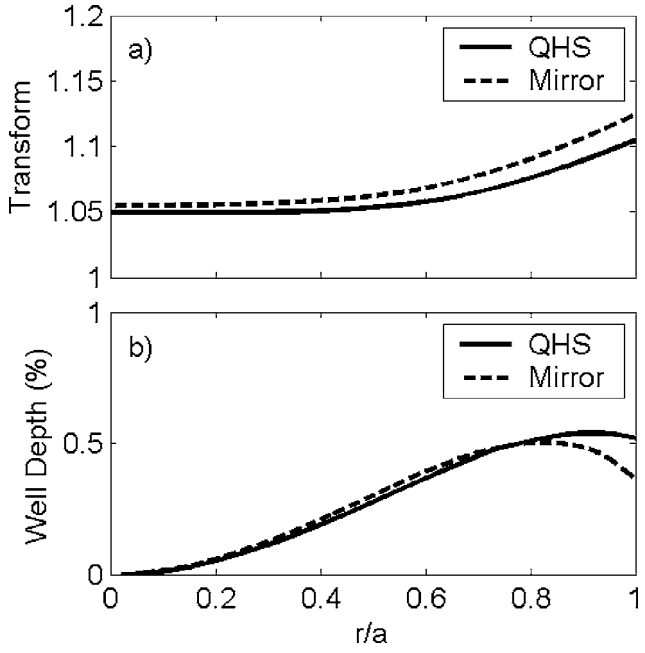

FIG. 3. Profiles of (a) rotational transform and (b) magnetic well depth for the QHS (solid line) and Mirror (dashed lines) configurations.

one field period (plus signs indicate that the current in the auxiliary coil is in the same direction as the main coils, minus signs indicate that it is in the opposite direction). In this table, "Mirror" refers to the nonsymmetric configuration that is studied in this paper. Results from the "Old Mirror 1" configuration are discussed in Refs. 17 and 21, and data from the "Old Mirror 2" configuration are shown in Ref. 22. For reference, the ECRH is launched at the beginning of a field period, i.e., just before coil number 1 in the table. An important feature of this particular Mirror configuration is that at the location where the ECRH power is injected into the torus and also where the Thomson scattering measurements are performed, the magnetic axis in Mirror is calculated to be within 1 mm of its location in QHS. In the past, the auxiliary coils were configured differently to break the quasisymmetry. In the old nonsymmetric configurations, the axis shifted 1–2 cm compared to QHS, which either changed the power deposition profile or made it impossible to make core measurements with the Thomson scattering system.[22] These problems have been alleviated due to the small axis shift in the new Mirror configuration, so that on-axis heating and on-axis Thomson scattering measurements can be performed simultaneously.

TABLE I. Distribution of auxiliary coil currents for one field period in the nonsymmetric configurations. Plus signs (+) indicate that the current in the auxiliary coil is in the same direction as the main coils, minus signs (–) indicate that it is in the opposite direction.

Coil Number	1	2	3	4	5	6	7	8	9	10	11	12
Mirror	–	+	+	+	–	–	–	–	+	+	+	–
Old Mirror 1	+	+	+	–	–	–	–	–	–	+	+	+
Old Mirror 2	+	+	+	+	+	+	–	–	–	–	–	–

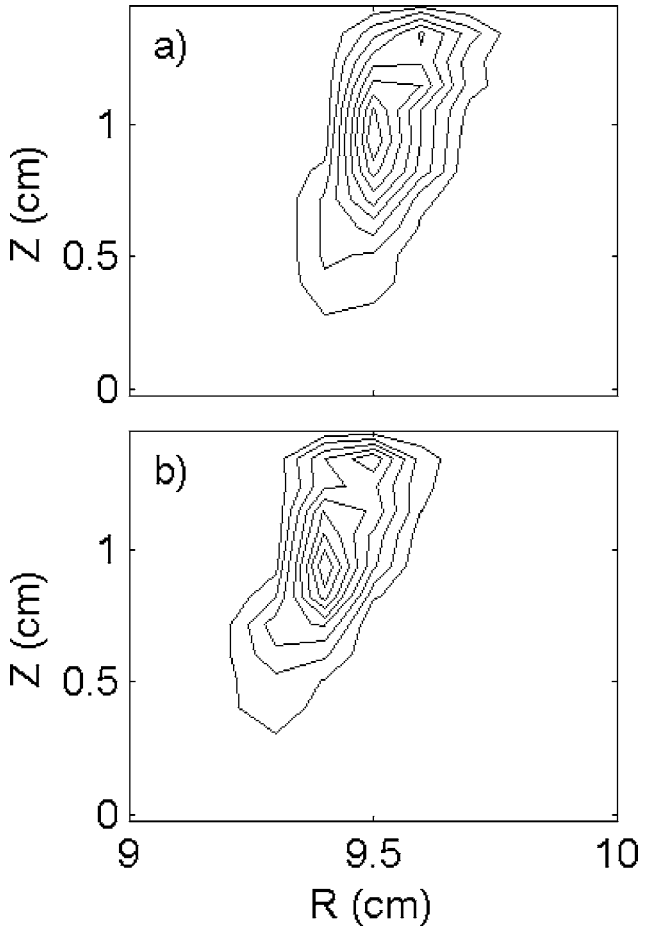

FIG. 4. Contours of the fraction of the electron current collected on the back of the head of the axis-finding probe for the (a) QHS and (b) Mirror configurations.

The small axis shift has been confirmed by measurements using an electron beam probe. The probe consists of an emission filament, which directs a beam of electrons along a magnetic field line, and a collection plate on the other side of the probe head. When the probe head is located on the magnetic axis, electrons travel around the torus and strike the collector plate after one transit of the machine. The magnetic axis is located with this probe by positioning it so that the fraction of emitted current that is collected at the back of the probe head is maximized. The collector is placed behind a shield with a 1 mm hole, determining the precision to which the axis can be located. In Fig. 4, contours of the collected fraction are shown for the two configurations. It can be seen that the location of maximum collected current in the Mirror configuration is within ~1 mm of the QHS case, verifying the small axis shift.

III. NEOCLASSICAL TRANSPORT CALCULATIONS

The neoclassical transport properties of HSX have been assessed using the drift kinetic equation solver (DKES).[23,24] DKES calculates the monoenergetic diffusion coefficient for a given magnetic configuration as a function of collisionality and radial electric field. Results of these calculations are shown in Fig. 5 for both the QHS and Mirror configurations,

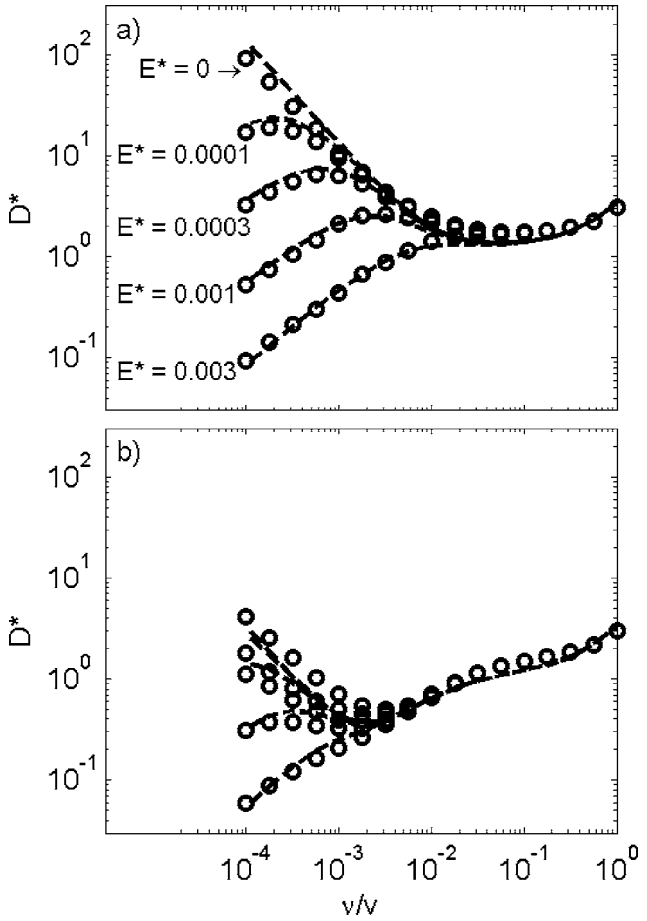

FIG. 5. The normalized monoenergetic diffusion coefficients ($D^* = D/[v_t(Bv_t/\Omega)^2K^{3/2}/2]$, where K is the particle energy) for (a) Mirror and (b) QHS, shown as a function of collision frequency normalized to the particle speed v. DKES calculations are shown as points, and fits based on Eq. (2) in the text are shown as lines. The different lines for each configuration represent calculations for different values for the radial electric field. The normalized electric fields ($E^* = E_r/v$) for the Mirror calculations are labeled; the QHS calculations use the same values.

at a normalized plasma radius of $r/a=0.5$. The normalizations used in this graph are the same as those used in Ref. 25. For a given collisionality, the transport coefficient is reduced by the radial electric field. In the figure, the different branches for each configuration are the results of calculations using different electric fields.

The diffusion coefficients from DKES are fit to an analytic form, which includes the $1/\nu$, $\nu^{1/2}$, and ν collisionality dependences in the long mean free path regime.[26] The form of this fit for the low collisionality transport is

$$\frac{1}{D} = \frac{1}{D_{1/\nu}} + \frac{1}{D_{\sqrt{\nu}}} + \frac{1}{D_{\nu}}, \tag{2a}$$

$$D_{1/\nu} = C_1 v_d^2 \frac{(2\varepsilon_{eff})^{3/2}}{\nu}, \tag{2b}$$

$$D_{\sqrt{\nu}} = C_2 v_d^2 \frac{\sqrt{\nu}}{|\Omega_E|^{3/2}}, \tag{2c}$$

$$D_{\nu} = C_3 \left(\frac{v_d}{\Omega_E}\right)^2 \nu, \tag{2d}$$

where v_d is the particle drift velocity, given by $v_d = K/B_0R_0$, with K the particle kinetic energy, q the particle charge, B_0 the magnetic field strength, and R_0 the plasma major radius. Ω_E in Eq. (2) is E_r/rB_0, where r is the minor radius and E_r the radial electric field, and C_1, C_2, and C_3 are fit parameters. This method of fitting the analytic expressions to the calculated DKES coefficients allows for the fast interpolation of the DKES results. The results of this procedure are shown in Fig. 5, where the dashed lines are the fit to the DKES calculations.

The neoclassical particle and heat fluxes are given by

$$\Gamma_s = -n_s\left[D_{11}^s\left(\frac{\nabla n_s}{n_s} - \frac{q_s E_r}{T_s}\right) + D_{12}^s \frac{\nabla T_s}{T_s}\right], \tag{3a}$$

$$Q_s = -n_s T_s\left[D_{21}^s\left(\frac{\nabla n_s}{n_s} - \frac{q_s E_r}{T_s}\right) + D_{22}^s \frac{\nabla T_s}{T_s}\right], \tag{3b}$$

where the subscript s denotes particle species. The coefficients D_{11}, D_{12}, D_{21}, and D_{22} are formed by integrating the monoenergetic diffusion coefficient over a Maxwellian with different energy weightings.[23]

The electric field is calculated from the ambipolarity condition of the neoclassical particle fluxes

$$\Gamma_e = \sum_i Z_i \Gamma_i. \tag{4}$$

Since HSX plasmas use hydrogen as the working gas, a single ion species with $Z=1$ is considered. Both the fluxes and the diffusion coefficients are functions of the radial electric field, making Eq. (4) a nonlinear function of E_r. Typically up to three solutions to the ambipolarity constraint may exist: the ion root, with a small negative or positive electric field, the electron root, which has a large positive field, and an unstable third root.[6] In HSX plasmas, the electron temperature is much larger than the ion temperature [T_e is typically 0.5–1.0 keV, whereas T_i is 20–30 eV (Ref. 17)]. Because of this, in the Mirror configuration the electron flux at zero electric field is larger than the ion flux, and only the electron root exists as a solution of Eq. (4). The resulting large electric field greatly reduces the transport in the Mirror configuration compared to the particle and heat flux that would result if the electric field were in the ion root.

IV. PARTICLE TRANSPORT

The particle source rate density has been calculated for HSX plasmas using the DEGAS code,[27] which uses a Monte-Carlo technique to calculate the distribution of neutrals in the plasma. The full three-dimensional geometry of HSX is input to the DEGAS code, along with the profiles of electron density and temperature, which are measured with a ten-channel Thomson scattering system.[28] The gas valve used to fuel HSX plasmas is included in the modeling as a localized gas source at the vessel wall. The locations where field lines outside of the last closed magnetic surface strike the wall have been calculated for the different magnetic configura-

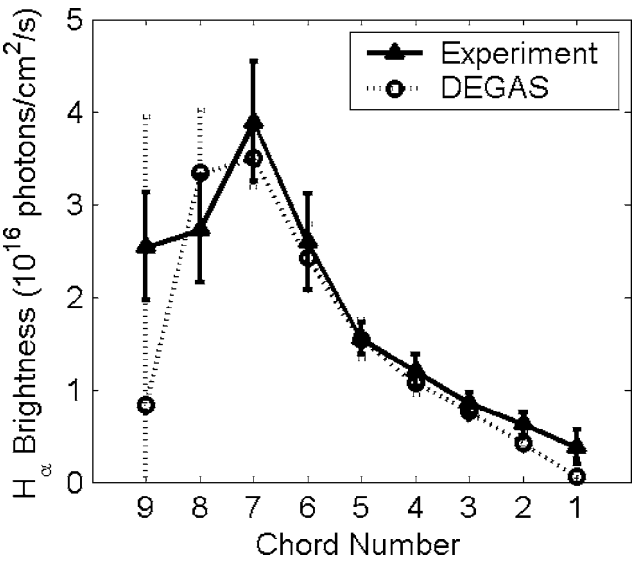

FIG. 6. H_α brightness across the plasma cross section from measurement (solid lines) and from calibrated DEGAS calculations (dashed). Chord number 5 is used to scale the DEGAS results to experiment.

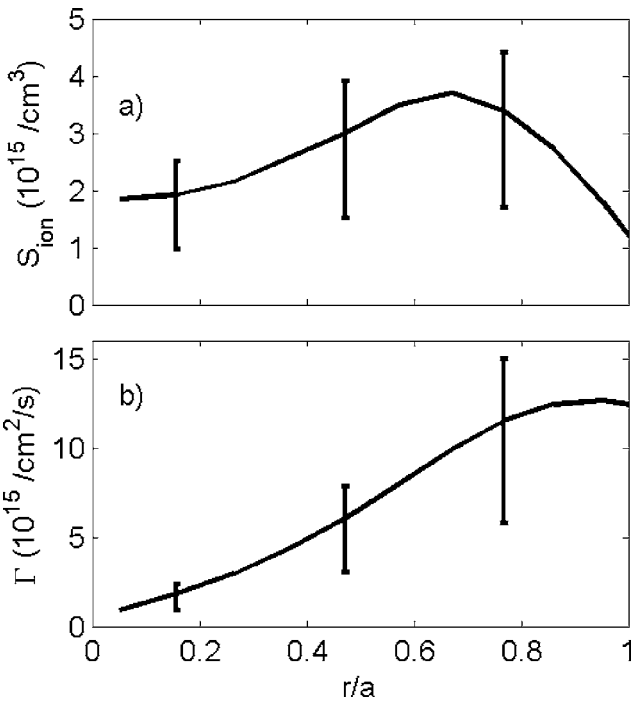

FIG. 7. Profiles of (a) particle source rate density and (b) radial particle flux for a QHS plasma, from DEGAS calculations and H_α measurements.

tions. The effect of particles recycling from the vessel wall has been modeled in DEGAS by means of a separate gas source localized to these strike points. Separate DEGAS runs are performed for the fueling due to the gas valve and that due to recycling.

The DEGAS calculations have been coupled to measurements using a suite of absolutely calibrated H_α detectors.[29] The H_α detectors are distributed in a toroidal array, which is distributed around the machine, and a poloidal array that covers the plasma cross section. The DEGAS calculations using the modeled recycling gas source are first calibrated by numerically integrating the H_α emission at a detector that is two field periods away from the gas valve. The DEGAS results are then scaled so that the simulated H_α brightness matches the measured value, giving the fueling due to recycling from the vessel wall. A similar technique is used to calibrate the DEGAS results for the portion of fueling due to puffing from the gas valve, using the measured and calculated brightness from a single H_α detector located near the gas puff. The resulting profiles of H_α brightness from DEGAS using this single-point normalization show good agreement with the measured profiles for both the toroidal and poloidal arrays, as shown in Fig. 6. The error bars in this figure indicate the relative uncertainty between the detectors in the measurements of H_α brightness. An additional uncertainty due to wall reflections arises in the factor used to scale the DEGAS results to match experiment. This method of scaling the DEGAS results using absolutely calibrated H_α measurements gives the particle source rate density in absolute units, which is then integrated to give the average radial particle flux as a function of minor radius, as is shown in Fig. 7. In this figure, the error bars include the uncertainty in the scale factor.

The measured density and temperature profiles for plasmas made in the QHS and Mirror configurations are shown in Fig. 8. These plasmas were heated with 80 kW of injected ECH power. As can be seen from this figure, the electron temperature is substantially higher in the QHS configuration than in Mirror (~1050 versus 750 eV). In addition, the den-

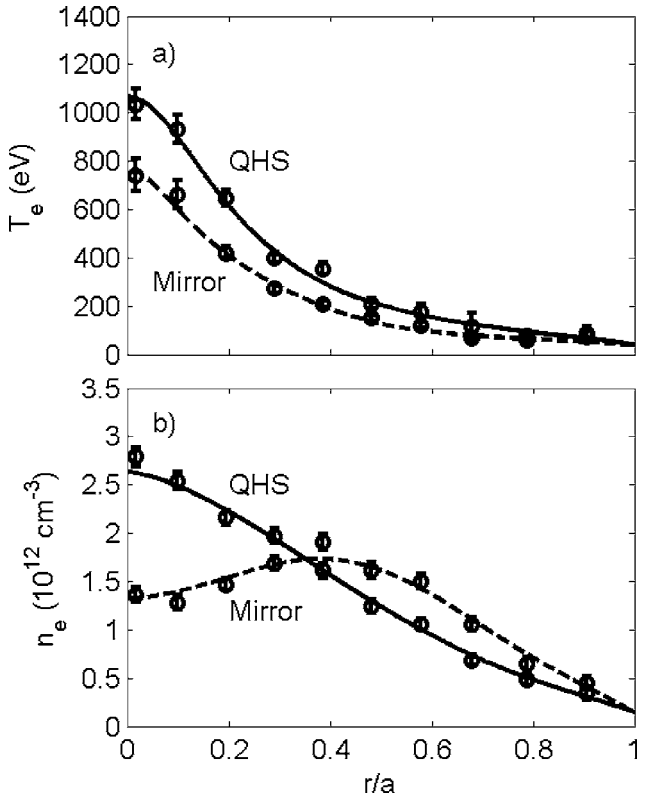

FIG. 8. Profiles of (a) electron temperature and (b) density in QHS and Mirror plasmas with 80 kW ECRH.

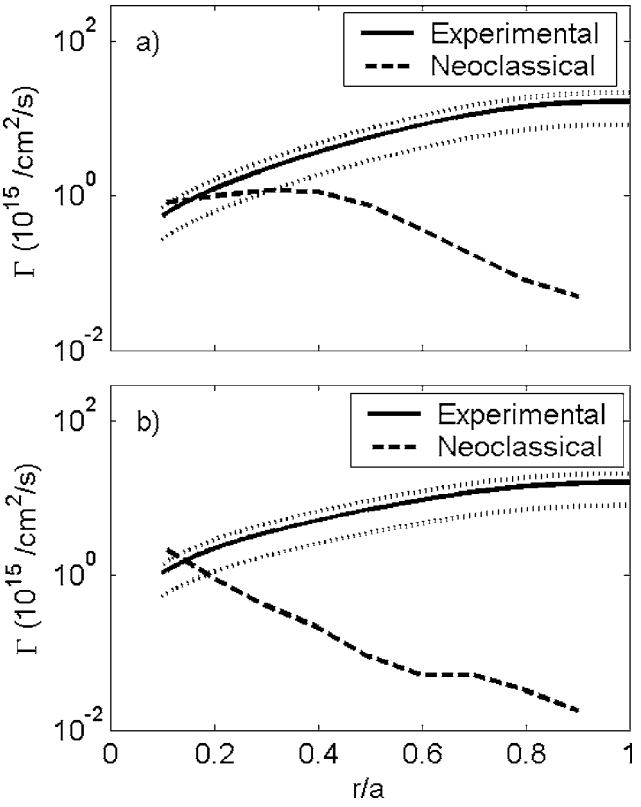

FIG. 9. Profiles of experimental (solid line) and neoclassical (dashed line) particle fluxes for the (a) Mirror and (b) QHS discharges of Fig. 8. The dotted lines represent the range of uncertainty in the experimental particle flux.

sity profile in QHS is centrally peaked, compared to a hollow profile in the core of the Mirror configuration.

Hollow density profiles such as that seen in the Mirror configuration are routinely observed in conventional stellarators heated with ECRH that is resonant with the field at the magnetic axis.[30] A hollow profile requires an outward convective particle flux in the core to be supported in steady state. To study what causes this profile shape, the experimental particle flux, as inferred from the H_α measurements and neutral modeling, is compared to the neoclassical particle flux. The experimental and neoclassical fluxes for the Mirror discharge parameters of Fig. 8 are displayed in Fig. 9(a). The uncertainty in the experimental particle flux is represented by the dotted line; the uncertainty in the neoclassical flux (based on the error in the measured density, electron temperature, and ion temperature) is ~10%. Inside a normalized radius of ~0.3, the particle flux is in agreement with the neoclassical value to within the error of the measurement. This corresponds to the region in which the density profile is hollow. The neoclassical particle flux in the Mirror case is dominated by that driven by the temperature gradient. Since the density gradient drives particles inward in this region, the outward directed flux is entirely driven by thermodiffusion. These results show that the hollowing out of the density profile observed in the Mirror configuration is caused by neoclassical thermodiffusion, which can drive particle flux up the density gradient in the core.

For the case of the QHS plasma, the peaked density profile can be understood in terms of the reduced neoclassical transport. Figure 9(b) shows the neoclassical and experimental particle fluxes for the QHS case. As the figure shows, the neoclassical particle flux (which is dominantly thermodiffusive) is much less than the experimental over most of the plasma minor radius; at a radius of $r/a=0.3$, the neoclassical flux is an order of magnitude less than the experimental value. At this location, the neoclassical diffusion coefficient D_{12}, which is associated with the thermodiffusive particle flux [see Eq. (3a)], is reduced a factor of 5 in QHS compared to Mirror. Thus, neoclassical thermodiffusion is not large enough to cause a hollow density profile, but has been reduced to a level such that anomalous transport dominates the particle flux. This results in a density profile that is centrally peaked, in strong contrast to the hollow density profile observed not only in the Mirror configuration, but also typically seen in conventional stellarators with on-axis ECRH.

V. ELECTRON THERMAL TRANSPORT

The higher electron temperature in the QHS plasma indicates a reduction in electron heat transport, if it is assumed that the absorbed power is similar in the two configurations. For a better comparison, however, plasmas have been produced in the QHS and Mirror configurations with similar temperature profiles and as close to the same density profile as possible. This is done in order to make a clear comparison of the transport in the two configurations to the neoclassical predictions. For discharges with different electron temperatures, such as those shown in Fig. 8, any dependence of the anomalous transport on temperature could make such a comparison difficult. To overcome this, the power has been varied between the two configurations in order to produce similar temperature profiles. This requires 2.5 times the injected power in the Mirror configuration as in QHS. Figure 10 shows the profiles for QHS plasmas with a launched power of 26 kW, and Mirror plasmas with 67 kW. Note that the density profiles cannot be matched in exactly the same way, due to the higher thermodiffusive flux in Mirror.

The total power absorbed by the plasma in these discharges has been measured using the Thomson scattering system. To do this, many similar discharges were taken, varying the time at which the Thomson measurement is made from just before to just after the turn-off of the ECRH power. At each point in time, the density and temperature profile is constructed from an average of 5–10 discharges. The profile is integrated over the volume to obtain the total kinetic stored energy. The absorbed power is then obtained from the time dependence of the stored energy according to

$$P_{\mathrm{abs}} = dW/dt(t = t_0^-) - dW/dt(t = t_0^+), \tag{5}$$

where W is the plasma stored energy, and t_0 is the time at which the ECH power is switched off. For the discharges being discussed, the plasma is in steady-state before the ECH turn-off, and so only the rate at which the energy drops when the power is turned off is used to determine the absorbed power. An example of this method is shown in Fig. 11, which shows the kinetic stored energy decay after ECH turn-off, along with a linear fit to the data that gives dW/dt. The

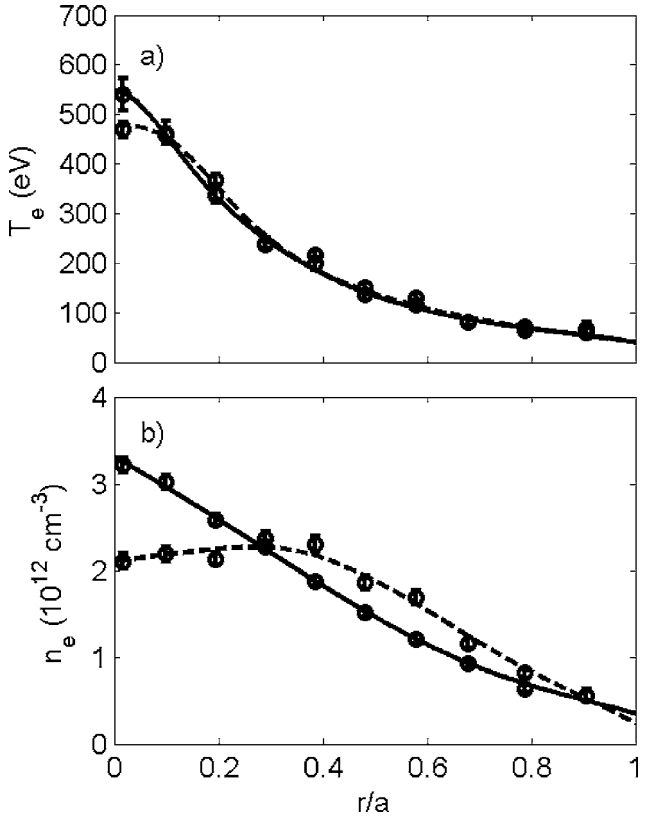

FIG. 10. Profiles of (a) electron temperature and (b) density for a QHS (solid line) plasma with 26 kW of injected power and a Mirror (dashed line) plasma with 67 kW of power.

variance in the slope of the linear fit to the data gives the error in the measurement of the absorbed power.

The absorbed power is also routinely measured on HSX using the same method, but with the stored energy measured with a diamagnetic loop. The reason for using the Thomson scattering method rather than the diamagnetic loop method is that the diamagnetic stored energy is often contaminated by the presence of a high-energy electron tail.[31] This population can dominate the total stored energy and absorbed power, especially at higher launched power. Since the Thomson scattering measurements are less sensitive to the high-energy tail, they are a better measurement of the bulk energy and absorbed power. Measurements of hard x rays from the suprathermal electrons have been made on HSX.[32] These measurements, along with data from the diamagnetic loop, indicate that the superthermal electrons are in the energy range of 15–50 keV. At these energies, the slowing down time of the tail is ~10–50 ms. Based on these slowing down times and estimated tail parameters, the power transferred from the tail to the bulk is 150–800 W. Since this is only ~5% of the ECRH power directly absorbed by the bulk, the power coupling between the tail and the bulk is neglected in this paper.

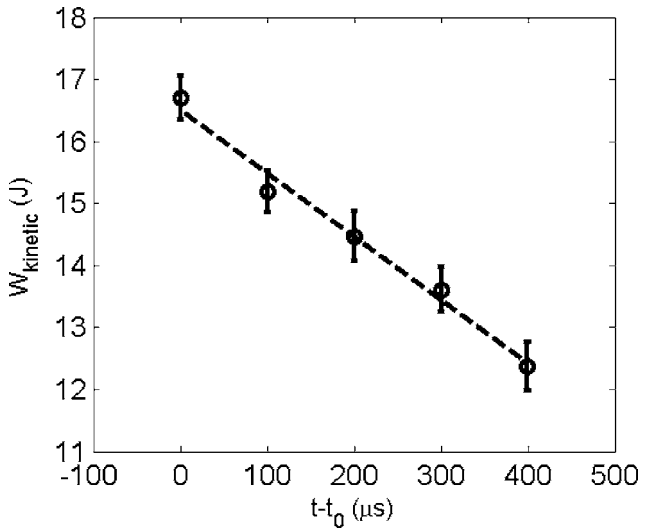

FIG. 11. Measured kinetic stored energy vs time for a QHS plasma with 26 kW of heating (t=0 is ECH switch-off). Line is fit to data that give absorbed power of 10±1.2 kW.

In the low-power QHS discharges, the tail population is relatively small; the absorbed power thus measured is 10.2 kW (±1.2 kW), compared to the diamagnetic value of 15 kW. In the high-power Mirror discharge, where the tail population is larger, the absorbed power from the Thomson scattering method is 15.0 kW (±1.3 kW), compared to 38 kW from the diamagnetic loop. The kinetic stored energy in both configurations is 17 J, giving bulk confinement times of 1.7 ms for the QHS plasma and 1.1 ms for Mirror. The confinement times measured using only the diamagnetic loop are 1.4 ms for QHS and 750 μs for Mirror. Thus, although the absolute value of the confinement time depends on how the contribution from suprathermal electrons is treated, the result that the confinement time in QHS is substantially longer than in Mirror is robust. Note that the tail represents a much larger potential power source in the Mirror case than in QHS, based on the diamagnetic measurements. Hence, the approach taken in this paper of neglecting tail-bulk coupling is a conservative measurement of the improvement of confinement in the QHS configuration.

The bulk electron heat transport has been analyzed for the QHS and Mirror plasmas shown in Fig. 10. In this analysis, the total power is taken from the measurements made with the Thomson scattering system, and ray-tracing calculations have been performed to obtain the shape of the power absorption profile.[31,33,34] The ray-tracing calculations consider single-pass absorption on the bulk plasma, with density and temperature profiles taken from the Thomson scattering measurements. Previous results indicate that taking multiple passes into account has little effect on the calculated power absorption.[31] Results of these calculations are shown in Fig. 12. As can be seen from this figure, the calculations show very centrally peaked power deposition, with absorption localized to within a normalized radius of ~0.2. The calculations also show negligible difference in the shape of the power deposition profile between the QHS and Mirror cases. The total absorbed power from the ray-tracing calculations is similar to that measured using the Thomson scattering system: 9 kW in the QHS case and 14 kW in Mirror. The agreement between the measurement and the calculations supports the assumption that the suprathermal electrons make only a small contribution to the power absorbed by the bulk. The power deposition profile used in the transport analysis is a fit to the ray-tracing calculations, with the same shape used for

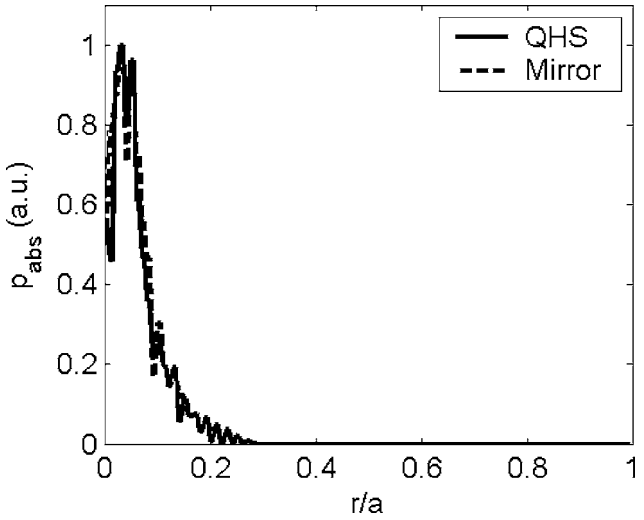

FIG. 12. Power deposition profiles from ray-tracing calculations for QHS and Mirror.

both configurations, and the total absorbed power level measured as described above. The analysis is performed in terms of the effective electron thermal diffusivity, which is calculated as

$$\chi_e = -\frac{q_e}{n_e \nabla T_e}. \tag{6}$$

This analysis neglects the effects of radiation, electron-ion coupling, and convection, as these terms are all small in the plasma core. These effects can become important outside a minor radius of $r/a \sim 0.6$, where convection especially can make up a significant part of the electron power balance. However, these terms change very little between the QHS and Mirror configurations, so that the effective diffusivity remains a useful means of comparing transport in this region.

The results of this analysis are shown in Fig. 13, where profiles are shown of the experimental electron thermal diffusivity χ_e. The error bars, indicated by the shaded regions, are taken from both the error in the measurement of the temperature profiles and the error in the kinetic measurement of the absorbed power. It can be seen from this figure that heat transport in the core of the QHS plasma is significantly reduced as compared to the Mirror case. At a radius of $r/a \sim 0.2-0.3$, where the temperature gradient is well determined, the value of χ_e is just above 2 m^2/s in QHS and ~ 4 m^2/s in Mirror. Also shown in Fig. 13 are the neoclassical values of the thermal diffusivity. This is the coefficient D_{22} from Eq. (3b), which is the dominant part of the neoclassical heat flux. The uncertainty in the neoclassical values, due to error in the measured density and electron and ion temperatures, is $\sim 10\%$ for both configurations. The magnitude of the reduction in the experimental χ_e in QHS compared to Mirror is comparable to the reduction in the neoclassical value, which is ~ 2.5 m^2/s at $r/a=0.3$. Toward the plasma edge, where the neoclassical transport is small, the two configurations have similar values of χ_e. In this region, anomalous transport is dominant, and the error in the measurement is too large to determine whether the quasisymmetric field has an effect on the anomalous transport.

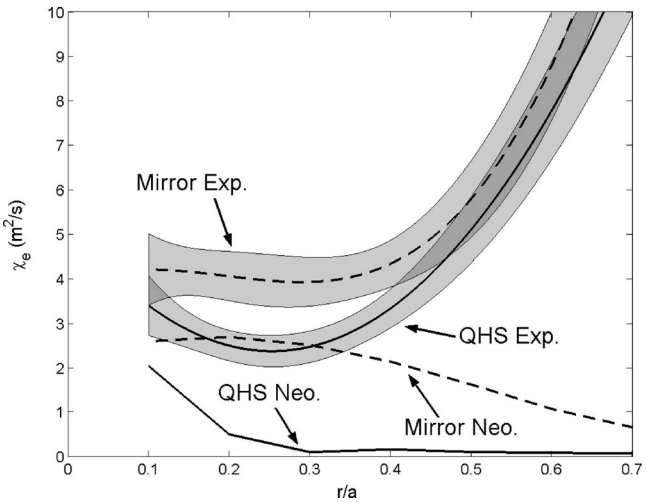

FIG. 13. Experimental and neoclassical thermal diffusivities for the discharges shown in Fig. 10.

VI. SUMMARY

Profiles of the electron density have been presented for plasma in the QHS and Mirror configurations. Transport analysis has been performed to study differences in these profiles. The particle source rate density has been obtained using 3D neutral gas modeling coupled to absolutely calculated H_α measurements. The resulting experimental radial particle flux is comparable to the neoclassical flux in the Mirror configuration. Thermodiffusion is the dominant component of the Mirror neoclassical particle flux, and causes the density profile to be hollow in the core. In the QHS configuration, the neoclassical thermodiffusive flux is reduced due to the quasisymmetric magnetic field, resulting in a centrally peaked density profile.

Electron temperature measurements have also been presented, showing that QHS plasmas are hotter than Mirror for the same input power. Transport analysis has been performed on discharges where the power levels in the two configurations are adjusted to give similar temperature profiles. This analysis shows that the QHS configuration has substantially lower electron heat transport in the plasma core. The magnitude of this reduction is comparable to the neoclassical prediction, demonstrating improved electron heat confinement with quasisymmetry.

ACKNOWLEDGMENTS

The authors would like to thank L. Owen, D. Spong, S. P. Hirshman, and Oak Ridge National Laboratory for providing the DEGAS and DKES codes. We also gratefully acknowledge the assistance of C. Deng, W. Guttenfelder, M. Frankowski, E. Jolitz, A. Piccione, and P. Probert.

This work was supported by the U.S. Department of Energy under Contract No. DE-FG02-93ER54222.

[1] A. A. Galeev and R. D. Sagdeev, in *Reviews of Plasma Physics*, edited by M. A. Leontovich (Consultants Bureau, New York, 1977), Vol. 7, p. 307.
[2] H. E. Mynick, Phys. Plasmas **13**, 058102 (2006).
[3] H. E. Mynick, T. K. Chu, and A. H. Boozer, Phys. Rev. Lett. **48**, 322 (1982).
[4] O. Motojima, N. Ohyabu, A. Komori *et al.*, Nucl. Fusion **43**, 1674 (2003).
[5] H. Wobig, H. Massberg, and H. Renner, W7-A Team, ECRH Group, and NI Group, in *Proceedings of the 11th International Conference on Plasma Physics and Controlled Nuclear Fusion Research, Kyoto, 1986* (International Atomic Energy Agency, Vienna, 1987), Vol. 2, p. 369.
[6] H. E. Mynick and W. N. G. Hitchon, Nucl. Fusion **23**, 1053 (1983).
[7] H. Idei, K. Ida, H. Sanuki *et al.*, Phys. Rev. Lett. **71**, 2220 (1993).
[8] H. Maassberg, C. D. Beider, U. Gasparino, M. Romé, and the W7-AS Team, Phys. Plasmas **7**, 295 (2000).
[9] F. Castejon, V. Tribaldos, I. Garcia-Cortes, E. de la Luna, J. Herranz, I. Pastor, T. Estrada, and the TJ-II Team, Nucl. Fusion **42**, 271 (2002).
[10] Y. Takeiri, T. Shimozuma, S. Kubo *et al.*, Phys. Plasmas **10**, 1788 (2003).
[11] J. Nuhrenberg and R. Zille, Phys. Lett. A **129**, 113 (1988).
[12] F. S. B. Anderson, D. T. Anderson, A. Almagri, P. G. Matthews, J. N. Talmadge, and J. L. Shohet, Fusion Technol. **27**, 273 (1995).
[13] J. N. Talmadge, V. Sakaguchi, F. S. B. Anderson, D. T. Anderson, and A. F. Almagri, Phys. Plasmas **8**, 5165 (2001).
[14] G. H. Neilson, M. C. Zarnstorff, J. F. Lyon, and the NCSX Team, J. Plasma Fusion Res. **78**, 214 (2002).
[15] D. A. Spong, S. P. Hirshman, L. A. Berry *et al.*, Nucl. Fusion **41**, 711 (2001).
[16] S. Gori, W. Lotz, and J. Nührenberg, *Theory of Fusion Plasmas* (Editrice Compositori, Bologna, 1997), p. 335.
[17] S. P. Gerhardt, J. N. Talmadge, J. M. Canik, and D. T. Anderson, Phys. Rev. Lett. **94**, 015002 (2005); Phys. Plasmas **12**, 056116 (2005).
[18] A. H. Boozer, Phys. Fluids **25**, 520 (1982).
[19] C. D. Beidler and W. N. G. Hitchon, Plasma Phys. Controlled Fusion **36**, 317 (1994).
[20] V. V. Nemov, S. V. Kasilov, W. Kernbichler, and M. F. Heyn, Phys. Plasmas **6**, 4622 (1999).
[21] J. N. Talmadge, K. M. Likin, A. E.-S. A. Abdou, A. F. Almagri, D. T. Anderson, F. S. B. Anderson, J. M. Canik, C. Deng, S. P. Gerhardt, and K. Zhai, Fusion Sci. Technol. **46**, 255 (2004).
[22] D. T. Anderson, A. Abdou, A. F. Almagri *et al.*, Fusion Sci. Technol. **50**, 171 (2006).
[23] S. P. Hirshman, K. C. Shaing, W. I. van Rij, C. O. Beasley, Jr., and E. C. Crume, Jr., Phys. Fluids **29**, 2951 (1986).
[24] W. I. van Rij and S. P. Hirshman, Phys. Fluids B **1**, 563 (1989).
[25] H. Sugama and S. Nishimura, Phys. Plasmas **9**, 4637 (2002).
[26] C. D. Beidler and W. D. D'haessleer, Plasma Phys. Controlled Fusion **37**, 463 (1995).
[27] D. Heifetz, D. Post, M. Petravic, J. Weisheit, and G. Bateman, J. Comput. Phys. **46**, 309 (1982).
[28] K. Zhai, F. S. B. Anderson, K. Willis, K. Likin, and D. T. Anderson, Rev. Sci. Instrum. **75**, 3900 (2004).
[29] S. P. Gerhardt, J. M. Canik, D. T. Anderson, and L. Owen, Rev. Sci. Instrum. **75**, 2981 (2004).
[30] H. Maassberg, R. Brakel, R. Burhenn *et al.*, Plasma Phys. Controlled Fusion **35**, B319 (1993).
[31] K. M. Likin, A. Abdou, A. F. Almagri *et al.*, Plasma Phys. Controlled Fusion **45**, A133 (2003).
[32] A. Abdou, Ph.D. thesis, University of Wisconsin, Madison (2005).
[33] R. C. Goldfinger, D. K. Lee, K. M. Likin, and B. D. Ochirov, Nucl. Fusion **31**, 2305 (1991).
[34] K. M. Likin and B. D. Ochirov, Sov. J. Plasma Phys. **18**, 42 (1992).